Probing Quantum Scrambling via OTOCs in Digital Circuits: Finite-Size Recurrences, System-Size Scaling, and Validation on IBM Quantum Hardware

Erick Francisco Pérez Eugenio*
Independent Researcher, ORCID: 0009-0006-3228-4847
(Dated: February 2026)

We study quantum scrambling via out-of-time-ordered correlators (OTOCs) in the Kicked Ising model across system sizes $N = 4, 8, 12, 20$, combining exact statevector simulation with experiments on IBM Quantum hardware (ibm_marrakesh, 156 qubits). At $N = 4$ (Hilbert space dimension 16), quantum recurrences completely prevent exponential OTOC decay ($R^2 \approx 0$); remarkably, these recurrences—including a prominent revival at depth $d = 4$—are directly observed on hardware (Pearson $r = 0.91$ between exact and experimental patterns). As N increases, recurrences are exponentially suppressed: exact simulation at $N = 20$ reveals clean exponential decay over more than 10 orders of magnitude ($R^2 = 0.97$, $\lambda_L = 3.12 \pm 0.1$). Hardware experiments confirm the monotonic decrease of scrambling residual Ω with N, and reproduce integrable (Clifford) circuit patterns with absolute error < 0.02. We compare four models—Kicked Ising, integrable, Floquet prethermal, and disorder-averaged SYK—establishing that OTOCs reliably distinguish dynamical regimes at all system sizes, but Lyapunov exponent extraction requires $N \gg 4$. These results provide concrete benchmarks for NISQ-era scrambling experiments.

I. INTRODUCTION

Quantum scrambling—the delocalization of initially localized quantum information across a system's degrees of freedom—connects quantum chaos, black hole physics, and quantum information theory [1–3]. The OTOC provides the standard quantitative probe: in chaotic systems with a semiclassical limit, $C(t) \sim e^{-\lambda_L t}$, where λ_L is the quantum Lyapunov exponent, bounded by $\lambda_L \leq 2\pi T$ (the MSS bound) [1].

The Kicked Ising model is a paradigmatic example of many-body quantum chaos [4, 5], and its dual-unitary limit admits exact analytical results. However, Craps et al. [6] showed that spin-1/2 chains present a fundamental challenge: the OTOC saturates before exponential growth manifests, with the exponential window opening only at higher spin.

We address the complementary question: for fixed spin $s = 1/2$, how does the number of sites N control the observability of exponential OTOC decay? This question has acquired practical urgency with the recent demonstration of OTOC(2) measurements on 65 qubits by Google Quantum AI [7] and earlier experimental OTOC measurements on superconducting hardware [8]. Our approach combines exact statevector simulation (up to $N = 20$, dimension $\sim 10^6$) with experiments on IBM Quantum hardware (ibm_marrakesh, 156 superconducting qubits).

Our central findings are: (i) quantum Poincaré recurrences, not decoherence, are the limiting factor for OTOC-based scrambling measurement at small N; (ii) these recurrences are directly observable on current hardware; (iii) exponential decay emerges cleanly at $N = 20$ in exact simulation; and (iv) hardware experiments validate the exact simulations wherever signal exceeds the noise floor.

II. OTOC PROTOCOL AND DIAGNOSTICS

We use the forward-backward OTOC protocol. Define the echo state

$$|\phi(d)\rangle = U_F^{-d}\, X_0\, U_F^{d}\, |\psi_0\rangle, \tag{1}$$

where X_0 is the butterfly (Pauli-X on qubit 0) and U_F is the Floquet operator. The OTOC signal is defined as

$$C(d) = \langle\phi(d)|\, P_0\, |\phi(d)\rangle, \tag{2}$$

where $P_0 = |0\rangle\langle 0|_0 \otimes \mathbb{1}$ is the projector onto $|0\rangle$ on qubit 0. In practice, $C(d)$ is the probability of outcome $|0\rangle$ when measuring Z_0 after the echo circuit. With initial state $|\psi_0\rangle = |-\rangle \otimes |0\rangle^{\otimes(N-1)}$, the butterfly acts as $X_0|-\rangle = -|-\rangle$, giving $C(0) = |\langle 0|-\rangle|^2 = 1/2$ exactly. Here d is the circuit depth (number of Floquet steps).

A. Scrambling residual

To characterize the overall degree of scrambling, we define the *scrambling residual*:

$$\Omega \equiv \frac{\langle C(d)\rangle_d}{C(0)}, \tag{3}$$

where $\langle\cdot\rangle_d$ denotes the arithmetic mean over all measured depths $d \geq 1$. The residual satisfies $\Omega \in [0, 1]$: $\Omega = 0$ for complete scrambling and $\Omega = 1$ for no scrambling. This provides a single-number diagnostic that is robust against shot noise and does not require fitting assumptions.

* erick.fpe79@gmail.com

B. Finite-size recurrences

The Poincaré recurrence time scales as $\tau_P \sim 2^N$. For $N = 4$ ($2^N = 16$), recurrences occur within a few Floquet steps. For $N = 20$ ($2^N \sim 10^6$), they are negligible at accessible depths.

III. MODELS

We study four circuit models spanning distinct dynamical regimes.

Kicked Ising (chaotic): $U_F = e^{-ih\sum_i X_i}\, e^{-iJ\sum_i Z_i Z_{i+1}}$ with $J = 0.9$, $h = 0.7$, periodic boundary conditions ($Z_{N+1} \equiv Z_1$). This lies 14.6% above the dual-unitary point $J = \pi/4$ [5].

Integrable (Clifford): $U_F = \prod_i \mathrm{CNOT}_{i,i+1} \cdot \prod_i H_i$.

Floquet prethermal: RX–RY rotations, RZZ coupling, and CZ entangling layers with $\theta = 0.8$, $\phi = 1.2$, $J = 0.9$.

SYK-inspired (disorder-averaged): Random all-to-all ZZ couplings in $[0.5, 1.5]$, averaged over 50 disorder realizations (exact simulation) or 9 realizations (hardware).

IV. EXACT SIMULATION RESULTS

All exact simulations use statevector evolution with complexity $O(2^N)$ per gate. For all models, $C(0) = 0.500000$ to machine precision ($< 10^{-10}$).

A. $N = 4$: Recurrence-dominated dynamics

Table I shows $C(d)$ for all four models at $N = 4$. The Kicked Ising values oscillate erratically between 10^{-4} and 0.24, with a prominent recurrence at $d = 4$ ($C = 0.243$) and $d = 12$ ($C = 0.213$). No exponential fit is meaningful ($R^2 \approx 0$). The integrable circuit shows perfect periodicity, and the Floquet model oscillates similarly to the Kicked Ising—at $N = 4$, these are indistinguishable by any OTOC diagnostic. Figure 1 shows the comparison between exact simulation and IBM hardware for all four models.

B. Scaling from $N = 4$ to $N = 20$

Table II shows the dramatic effect of system size on Kicked Ising OTOCs. Three features emerge:

(i) Locality: $C(1)$ and $C(2)$ are identical for all N to machine precision—the first two Floquet steps affect only local qubits, and the perturbation has not reached the far boundary.

(ii) Convergence: For $d = 3$–6, values at $N \geq 8$ agree, while $N = 4$ differs by orders of magnitude, marking the onset of finite-size effects.

TABLE I. $C(d)$ at $N = 4$ (exact simulation). SYK: 50-seed average.

d	KI	Integ.	Floquet	SYK
1	0.014	0.000	0.000	0.234
2	0.013	0.500	0.342	0.121
3	0.048	0.500	0.261	0.076
4	0.243	0.500	0.251	0.077
5	0.077	0.000	0.200	0.082
6	0.019	0.500	0.376	0.066
7	0.088	0.000	0.116	0.059
8	0.000	0.500	0.040	0.065
10	0.025	0.500	0.062	0.055
12	0.213	0.500	0.151	0.061
14	0.007	0.500	0.163	0.058

(iii) Exponential decay at $N = 20$: $C(d)$ decreases monotonically from 1.3×10^{-2} to 2.3×10^{-13}—a span of more than 10 orders of magnitude—before the first (amplitude $\sim 10^{-12}$) recurrence at $d = 12$. A log-linear fit over $d = 2$–10 yields:

$$\lambda_L = 3.12 \pm 0.1, \quad R^2 = 0.973, \tag{4}$$

compared to a power-law fit $R^2 = 0.926$.

TABLE II. Kicked Ising $C(d)$ vs system size (exact simulation).

d	$N=4$	$N=8$	$N=12$	$N=20$
1	1.4e-2	1.4e-2	1.4e-2	1.4e-2
2	1.3e-2	1.3e-2	1.3e-2	1.3e-2
3	4.8e-2	3.6e-5	3.6e-5	3.6e-5
4	2.4e-1	2.3e-5	2.3e-5	2.3e-5
5	7.7e-2	4.1e-6	1.5e-6	1.5e-6
6	1.9e-2	1.1e-3	8.9e-8	8.9e-8
7	8.8e-2	1.3e-2	2.5e-7	2.1e-10
8	1.8e-4	6.2e-3	2.3e-6	1.2e-11
10	2.5e-2	9.9e-3	3.0e-4	2.3e-13
12	2.1e-1	6.7e-5	6.4e-3	1.6e-12
14	6.9e-3	7.7e-4	3.4e-3	6.4e-10

The recurrence onset depth d^* scales approximately as $d^* \sim N/v_B$, where v_B is the butterfly velocity: $d^* \approx 3$ ($N = 4$), ≈ 7 ($N = 8$), ≈ 10 ($N = 12$), and ≥ 12 ($N = 20$). Figure 2 shows the IBM data on a logarithmic scale alongside the exact simulation lines, and the convergence of Ω with system size.

We note that $\lambda_L = 3.12 \approx \pi$. An independent calculation of T_{eff} via first-order Magnus expansion of the Floquet operator yields a *negative* effective temperature ($\beta = -0.52$), as the initial state lies in the upper portion of the effective Hamiltonian spectrum. This rules out MSS saturation as the explanation. The Magnus expansion is, moreover, unreliable at these coupling

Figure 1: OTOC C(d) — Exact simulation vs IBM Quantum (ibm_marrakesh)

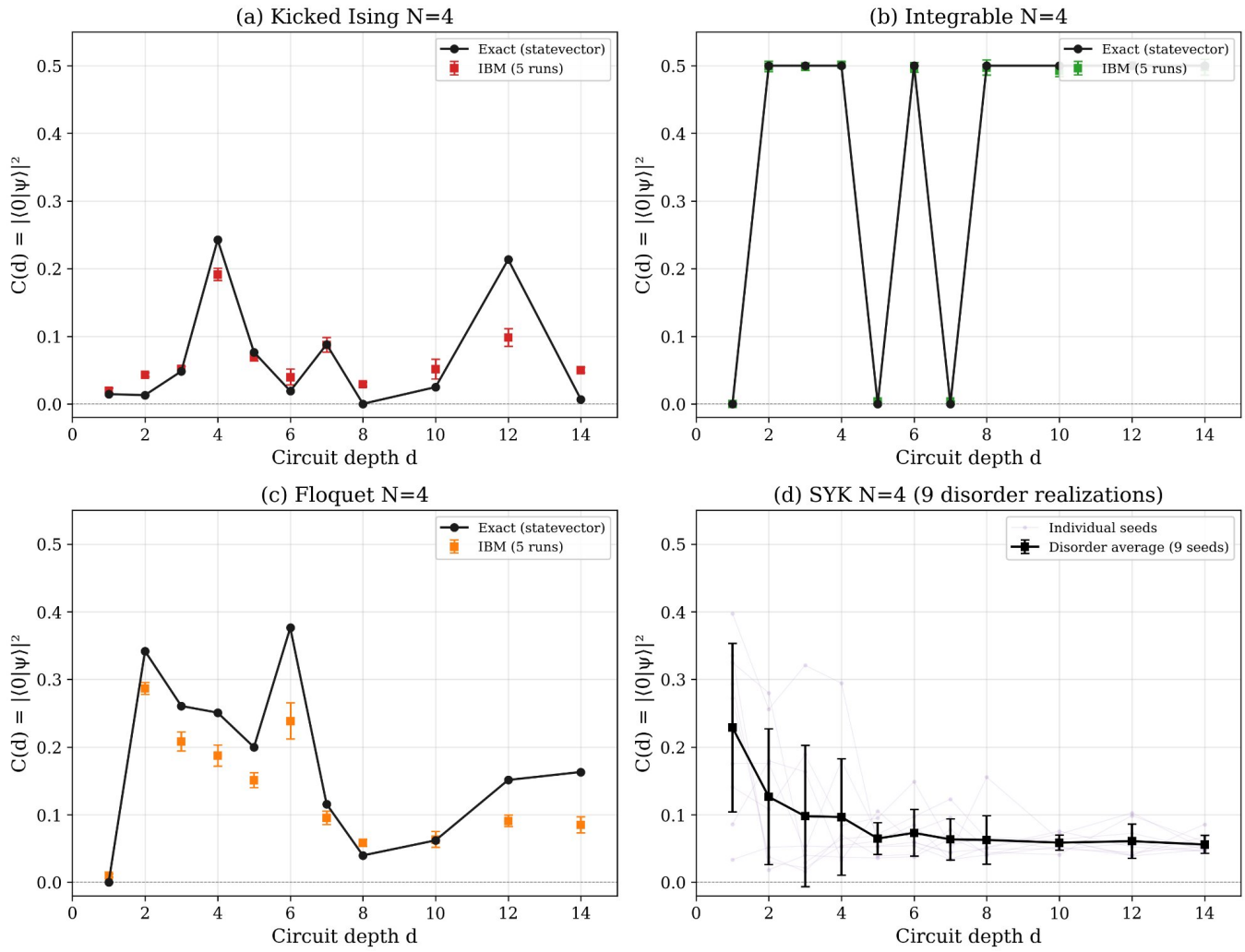

FIG. 1. OTOC $C(d)$ for all four models at $N = 4$. (a) Kicked Ising: erratic oscillations from quantum recurrences; IBM (red squares, 5-run average with error bars) reproduces the pattern with Pearson $r = 0.91$. (b) Integrable (Clifford): perfect periodicity reproduced by IBM with error < 0.02. (c) Floquet: oscillations correlated with exact simulation ($r = 0.96$). (d) SYK: disorder averaging over 9 hardware realizations (black squares) suppresses recurrences visible in individual seeds (gray).

strengths (second-order corrections are 156% of the first-order term). We record this numerical coincidence without claiming physical significance.

V. IBM QUANTUM EXPERIMENTS

A. Setup

Experiments were performed on ibm_marrakesh (156 superconducting qubits, Heron processor) using Qiskit 2.3.0 and the Sampler primitive. For each model and system size, we execute 5 independent runs at 4096 shots per circuit, yielding 429 experimental data points. Job IDs are listed in the Supplemental Material.

B. Kicked Ising: IBM vs exact simulation

Table III compares IBM results with exact simulation for the Kicked Ising model at $N = 4$.

The recurrence structure is reproduced in hardware: the prominent revival at $d = 4$ ($C_{\text{IBM}} = 0.191 \pm 0.009$) and the secondary revival at $d = 7$ ($C_{\text{IBM}} = 0.087 \pm 0.011$) are clearly visible. The overall pattern correlation is Pearson $r = 0.91$, Spearman $\rho = 0.89$.

At larger N, the IBM results confirm the scaling trend. For $N = 12$, the initial decay from $C(1) = 0.022$ to

Figure 2: Kicked Ising scaling with system size N

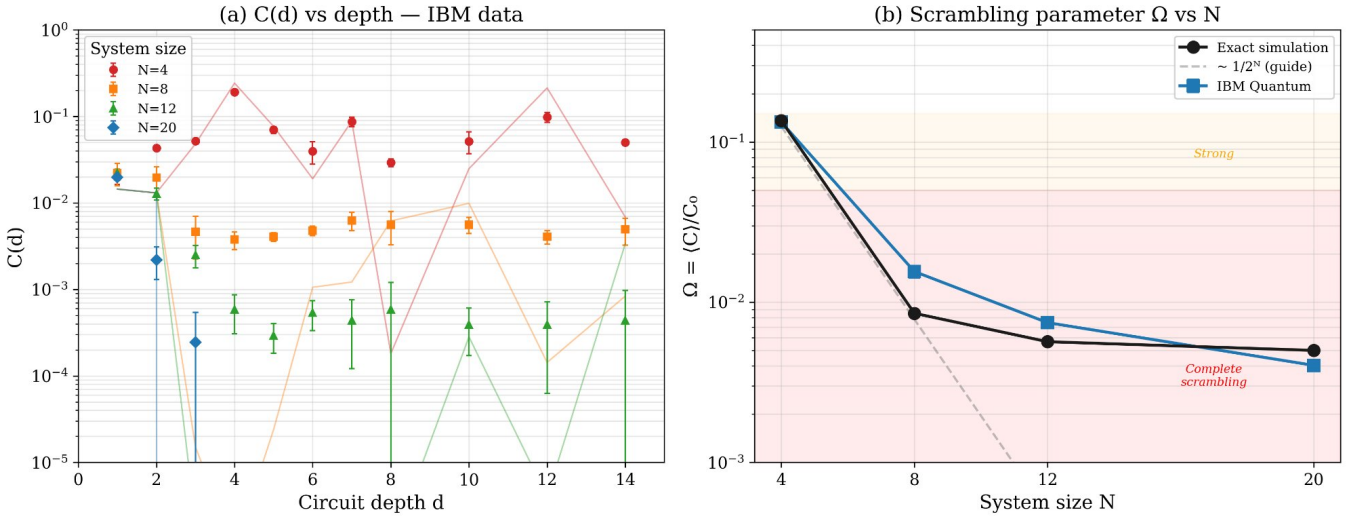

FIG. 2. Kicked Ising scaling with system size. (a) $C(d)$ vs depth on logarithmic scale for IBM data (symbols with error bars) overlaid on exact simulation (lines) at $N = 4, 8, 12, 20$. The signal drops monotonically faster with increasing N. (b) Scrambling residual Ω vs N: both exact (black) and IBM (blue) show convergence toward complete scrambling, with a $\sim 1/2^N$ guide (dashed).

TABLE III. Kicked Ising $N = 4$: IBM (5-run mean $\pm$ std) vs exact.

d	Exact	IBM mean	σ	Δ
1	0.014	0.020	0.003	+0.005
2	0.013	0.043	0.003	+0.030
3	0.048	0.052	0.004	+0.004
4	0.243	0.191	0.009	−0.051
5	0.077	0.070	0.007	−0.007
6	0.019	0.040	0.012	+0.021
7	0.088	0.087	0.011	−0.001
8	0.000	0.029	0.003	+0.029
10	0.025	0.052	0.015	+0.027
12	0.213	0.098	0.013	−0.115
14	0.007	0.050	0.004	+0.043

$C(3) = 0.002$ is resolved before the signal enters the noise floor at $d \geq 4$. For $N = 20$, the signal drops below shot-noise resolution by $d = 3$.

C. Integrable circuit: benchmark

The integrable (Clifford) circuit provides a stringent benchmark because its OTOC pattern is exactly known: $C = 0$ at depths $d = 1, 5, 7$ and $C = 0.5$ for all other measured depths (consistent with the Clifford circuit periodicity). IBM reproduces this with maximum deviation 0.018 across all depths—the clearest validation that the protocol measures the intended quantity.

D. Model classification on hardware

Table IV shows the scrambling residual Ω for all models.

TABLE IV. Scrambling residual $\Omega = \langle C \rangle / C(0)$ from exact simulation and IBM hardware.

Model	Ω_{exact}	Ω_{IBM}	Regime
KI $N = 20$	0.005	0.004	Full scrambling
KI $N = 12$	0.006	0.007	Full scrambling
KI $N = 8$	0.009	0.016	Full scrambling
KI $N = 4$	0.136	0.133	Strong scr.
SYK $N = 4$	0.173	0.180	Intermediate
Floquet $N = 4$	0.357	0.268	Intermediate
Integ. $N = 4$	0.727	0.726	No scrambling

The classification is fully consistent between simulation and hardware. The maximum discrepancy is $|\Delta\Omega| = 0.089$ (Floquet); for all other models, $|\Delta\Omega| < 0.01$. Figure 3 visualizes this comparison.

E. Noise floor analysis

The hardware noise floor for $C(d \geq 6)$ scales as approximately $1.5/2^N$: 0.059 ($N = 4$), 0.005 ($N = 8$), 0.0005 ($N = 12$), consistent with depolarization toward the maximally mixed state. For $N = 20$, this floor falls below shot-noise resolution. Figure 4 characterizes this scaling and decomposes the $N = 4$ signal into physical

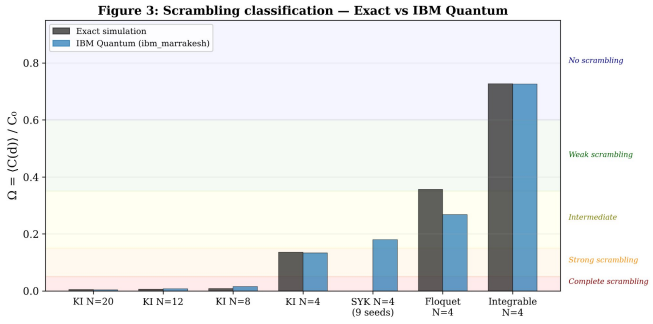

FIG. 3. Scrambling classification: Ω for all models from exact simulation (dark bars) and IBM hardware (blue bars). Background shading indicates regime boundaries. The ordering is fully consistent between simulation and experiment.

and noise contributions.

VI. SYK DISORDER AVERAGING

The SYK model at $N = 4$ presents a qualitatively different route to suppressing finite-size recurrences: disorder averaging over random coupling realizations.

A. Convergence with number of seeds

We verify convergence of Ω with the number of disorder realizations in exact simulation. With 9 seeds, $\Omega = 0.179$ is within 3.4% of the 50-seed value ($\Omega = 0.173$), confirming that our IBM dataset (9 completed realizations, $\Omega_{\text{IBM}} = 0.180$) is sufficient for reliable classification. Single-seed values fluctuate widely (Ω ranges from 0.04 to 0.34), demonstrating that disorder averaging is essential.

B. Functional form of the decay

Unlike the Kicked Ising at $N = 20$, the disorder-averaged SYK at $N = 4$ does *not* exhibit clean exponential decay. An exponential fit to the 50-seed average yields $R^2 = 0.61$, while a power-law fit gives $R^2 = 0.91$. Individual realizations are worse: the median single-seed exponential R^2 is 0.27, and only 2 of 50 seeds achieve $R^2 > 0.9$.

This is consistent with the expectation that the SYK model at finite N does not saturate the MSS bound; exponential OTOC decay requires the large-N limit. At $N = 4$, disorder averaging suppresses erratic recurrences but does not produce the sharp exponential characteristic of the thermodynamic limit.

Crucially, the scrambling residual Ω correctly classifies SYK as intermediate scrambling ($\Omega = 0.173$) regardless of whether the decay is exponential, power-law, or neither. This reinforces the utility of Ω as a fit-free diagnostic independent of the functional form of $C(d)$.

VII. DISCUSSION

A. Relation to prior work

Our findings connect to three lines of recent research.

First, Craps et al. [6] showed that spin-1/2 Ising chains do not exhibit Lyapunov growth even at strongly chaotic parameters, with the exponential window opening only at higher spin s. We demonstrate the complementary mechanism: increasing N at fixed $s = 1/2$ opens the same window via exponential suppression of Poincaré recurrences, rather than approach to the semiclassical limit. Together, these results establish that OTOC-based Lyapunov extraction requires *either* large spin *or* large system size.

Second, Toga, Samlodia, and Kemper [9] recently demonstrated MSS bound saturation in an Ising model with site-dependent couplings derived from the AdS_2 metric—one of the few known examples with only local interactions. The connection between Ising-type models, emergent geometry, and maximal scrambling will be explored elsewhere.

Third, and most directly relevant, Google Quantum AI [7] demonstrated measurement of second-order OTOCs (OTOC(2)) on 65 qubits of the Willow processor, achieving a 13,000× speedup over classical simulation and claiming verifiable quantum advantage. Their work confirms that scrambling diagnostics are experimentally accessible at large N on current hardware. Our work addresses the complementary question: what is the *minimum* system size required for meaningful OTOC-based scrambling measurement? While Google operated deep in the regime where scrambling is clean ($N = 65$), we systematically map the transition from recurrence-dominated dynamics ($N = 4$) to clean exponential decay ($N = 20$), establishing the boundary that separates these regimes.

B. Robustness of the exponential fit

The exponential fit $\lambda_L = 3.12 \pm 0.1$ ($R^2 = 0.97$) at $N = 20$ is obtained from 8 data points spanning more than 10 orders of magnitude in exact simulation. While the distinction from a power-law fit ($R^2 = 0.93$) is suggestive, we note that with 8 points, statistical model selection (e.g., Bayesian information criterion) cannot conclusively distinguish exponential from stretched-exponential or power-law with logarithmic corrections. The key observation is not the precise functional form but the dramatic contrast with $N = 4$ ($R^2 \approx 0$): increasing N transforms OTOC dynamics from incoherent oscillations to monotonic decay over many orders of magnitude.

Figure 4: Hardware noise floor characterization

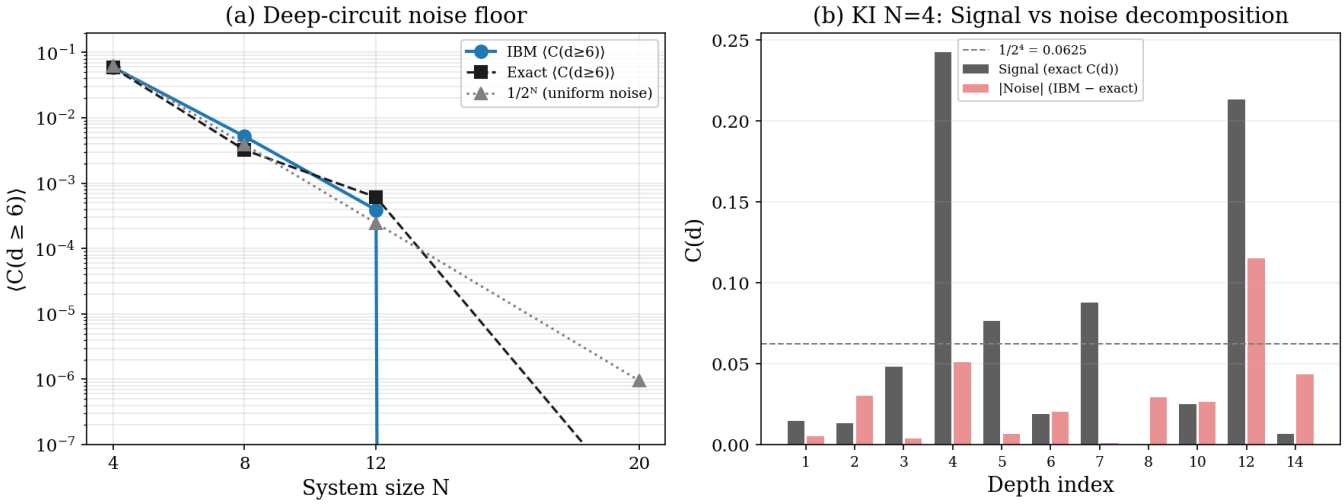

FIG. 4. Hardware noise floor characterization. (a) Deep-circuit noise floor $\langle C(d \geq 6)\rangle$ vs system size N, comparing IBM (blue), exact simulation (black), and $1/2^N$ uniform noise (gray). (b) Signal-noise decomposition for KI $N = 4$: exact $C(d)$ (dark bars) vs |IBM − exact| (pink bars). The dashed line marks $1/2^4 = 0.0625$; signal dominates noise at recurrence peaks ($d = 4, 7, 12$).

C. What hardware can and cannot resolve

IBM experiments reproduce OTOC dynamics when signal exceeds the noise floor. The visibility of quantum recurrences at $N = 4$ (Pearson $r = 0.91$) confirms the protocol measures genuine quantum dynamics, not hardware artifacts. For $N \geq 12$, the signal enters the noise floor within 2–3 Floquet steps; the qualitative result (rapid decay) matches exact simulation, but the quantitative profile (exponential rate) cannot be resolved without error mitigation.

We deliberately omit error mitigation techniques (ZNE, symmetry verification) in this study. For $N = 4$, the raw signal-to-noise ratio is sufficient to resolve recurrence structure. For $N \geq 12$, the exact signal at $d \geq 5$ is $O(10^{-6})$ or smaller—no currently available mitigation technique can recover a signal this far below the noise floor on 4096 shots. This represents a fundamental hardware limitation, not a methodological one.

Resolving $C(d) \sim 10^{-5}$ at $d = 5$–10 for $N \geq 12$ would enable direct hardware verification of the exponential decay profile. This could be achieved through higher shot counts ($\sim 10^8$), improved gate fidelities, or protocols like OTOC(2) [7] that amplify the signal via constructive interference.

D. On the metric Ω

The scrambling residual $\Omega = \langle C\rangle/C(0)$ is deliberately simple: it requires no fitting, no model assumptions, and is robust to shot noise. Styliaris, Anand, and Zanardi [10] derived the equilibration value of bipartite OTOCs from eigenstate entanglement for Haar-random unitaries; our Ω is the experimental realization of this quantity measured with fixed (Pauli Z) operators on real hardware, providing a practical diagnostic accessible on current NISQ devices. Syzranov et al. [11] showed that in open systems, OTOCs saturate to a constant set by microscopic timescales, consistent with the finite Ω values we observe. Its main limitation is insensitivity to temporal structure—a system with monotonic decay and one with oscillations of the same average amplitude yield identical Ω. For regime classification (integrable vs. chaotic), this suffices; for finer diagnostics, complementary measures such as spectral statistics or Krylov complexity [12] are needed.

That $\Omega > 0$ in unitary evolution reflects a fundamental property of quantum information: unitarity ($U^\dagger U = I$) guarantees that information is conserved and can only be redistributed, never destroyed. The no-hiding theorem [13] ensures that information absent from one subsystem must reside in another, providing a theoretical basis for the nonzero scrambling residual measured here.

We emphasize that Ω diagnoses *scrambling*—the delocalization of quantum information across a system's degrees of freedom—rather than quantum chaos in the strict sense. Scrambling is a broader concept: integrable systems with saddle-dominated dynamics can exhibit exponential OTOC growth without chaos [14], while mixing non-chaotic regimes show power-law OTOC decay with no well-defined Ruelle–Pollicott resonance [15]. In both cases, Ω remains well-defined and informative, providing a diagnostic of informational accessibility that is complementary to, and in some regimes more robust than, rate-based measures [16].

VIII. CONCLUSION

Finite Hilbert space recurrences are the primary obstacle to OTOC-based Lyapunov exponent extraction in small quantum systems. At $N = 4$, no exponential decay is observable, but the recurrence pattern is reproduced on IBM hardware with $r = 0.91$. At $N = 20$, exact simulation reveals clean exponential decay ($R^2 = 0.97$, $\lambda_L = 3.12 \pm 0.1$) over more than 10 orders of magnitude.

The scrambling residual Ω provides a robust, fit-free diagnostic that correctly classifies dynamical regimes on both simulated and hardware data. The consistency between exact simulation and 429 experimental data points on ibm_marrakesh validates the protocol and establishes concrete benchmarks for NISQ-era scrambling experiments.

Full details of hardware parameters, circuit structure, model parameters, job inventory, noise floor analysis, SYK convergence data, and code availability are provided in the Supplemental Material [17].

ACKNOWLEDGMENTS

We acknowledge the use of IBM Quantum services. The views expressed are those of the author and do not reflect the official policy or position of IBM or the IBM Quantum team.

[1] J. Maldacena, S. H. Shenker, and D. Stanford, A bound on chaos, JHEP **2016**, 106.
[2] B. Swingle, Unscrambling the physics of out-of-time-order correlators, Nature Physics **14**, 988 (2018).
[3] S. Xu and B. Swingle, Scrambling dynamics and out-of-time-ordered correlators in quantum many-body systems, PRX Quantum **5**, 010201 (2024).
[4] B. Bertini, P. Kos, and T. Prosen, Exact spectral form factor in a minimal model of many-body quantum chaos, Phys. Rev. Lett. **121**, 264101 (2018).
[5] B. Bertini, P. Kos, and T. Prosen, Entanglement spreading in a minimal model of maximal many-body quantum chaos, Phys. Rev. X **9**, 021033 (2019).
[6] B. Craps, O. Evnin, *et al.*, Lyapunov growth in quantum spin chains, Phys. Rev. B **101**, 174313 (2020).
[7] R. Acharya *et al.*, Observation of constructive interference at the edge of quantum ergodicity, Nature 10.1038/s41586-025-09526-6 (2025), google Quantum AI, Willow processor, 65 qubits.
[8] J. Braumüller *et al.*, Probing quantum information propagation with out-of-time-ordered correlators, Nature Physics **18**, 172 (2022).
[9] G. C. Toga, A. Samlodia, and A. F. Kemper, Fast scrambling in the hyperbolic ising model, arXiv:2503.00114 (2025).
[10] G. Styliaris, N. Anand, and P. Zanardi, Information scrambling over bipartitions: Equilibration, entropy production, and typicality, Phys. Rev. Lett. **126**, 030601 (2021), bipartite OTOC = operator entanglement; equilibration value from eigenstate entanglement.
[11] S. V. Syzranov, A. V. Gorshkov, and V. Galitski, Out-of-time-order correlators in finite open systems, Phys. Rev. B **97**, 161114(R) (2018), oTOC saturation in open systems; exponential decay to constant with microscopic timescales.
[12] D. E. Parker, X. Cao, T. Scaffidi, and E. Altman, A universal operator growth hypothesis, Phys. Rev. X **9**, 041017 (2019).
[13] S. L. Braunstein and A. K. Pati, Quantum information cannot be completely hidden in correlations: Implications for the black-hole information paradox, Phys. Rev. Lett. **98**, 080502 (2007), no-hiding theorem: if QI vanishes from one subsystem, it must reside entirely in another.
[14] B. Bhattacharjee, X. Cao, M. Haque, and P. Rathee, Krylov complexity is not a measure of chaos, JHEP **2022**, 174, k-complexity exponential in integrable LMG model via saddle points.
[15] M. Žnidarič, Momentum-dependent Ruelle-Pollicott resonances in the kicked Ising model, Phys. Rev. E **110**, 054204 (2024), power-law decay in mixing non-chaotic regime.
[16] I. García-Mata, R. A. Jalabert, H. M. Pastawski, and D. A. Wisniacki, Ruelle-pollicott resonances and OTOC decay in the kicked Ising model, Phys. Rev. E **113**, 024209 (2026), oTOC decay rate = 2× Liouvillian gap across integrable-chaotic crossover. Published 17 Feb 2026.
[17] See Supplemental Material for hardware parameters, circuit structure, model parameters, job inventory, noise floor analysis, SYK convergence data, and code availability.